Received: 16 September 2019 | Revised: 4 November 2019 | Accepted: 4 November 2019

DOI: 10.1111/jace.16900

ORIGINAL ARTICLE

Journal of the American Ceramic Society

Modeling birefringence in SiO_2 glass fiber using surface stress relaxation

Bronson D. Hausmann[1] | **Paul A. Miller**[1] | **Emily M. Aaldenberg**[1] | **Thierry A. Blanchet**[2] | **Minoru Tomozawa**[1]

[1]Department of Materials Science and Engineering, Rensselaer Polytechnic Institute, Troy, NY, USA

[2]Department of Mechanical, Aerospace & Nuclear Engineering, Rensselaer Polytechnic Institute, Troy, NY, USA

Correspondence
M. Tomozawa, Department of Materials Science and Engineering, Rensselaer Polytechnic Institute, Troy, NY. USA.
Email address: tomozm@rpi.edu

Present address
Paul A. Miller, Lincoln Laboratory, Massachusetts Institute of Technology, Lexington, MA, USA

Emily M. Aaldenberg, Corning Incorporated, Painted Post, NY, USA

Funding information
NSF, Grant/Award Number: DMR-1713670; Corning, Inc

Abstract

The retardance of silica glass fibers was evaluated using photoelastic techniques. Here, surface birefringence in glass fibers is shown to be a consequence of surface stress relaxation for as-received fibers drawn from Suprasil II. The surface features of the birefringent fibers were compared to a model of the residual axial stress profile resulting from a diffusion-controlled surface stress relaxation. Additionally, a uniform birefringence in the fiber equivalent to a constant tensile stress was recognized and attributed to structural anisotropy produced during fiber drawing. The contribution of structural anisotropy to the observed birefringence remained constant as the surface features were successively etched away. Surface compressive stress generation was also observed, as retardance corresponding to a surface compressive stress was found to increase with applied tensile stress during short heat treatments. Significant features of the retardance profile in as-received silica glass fibers, with a thin surface compressive stress layer and compensating interior tensile stress, agreed with the residual stress profiles predicted by the surface stress relaxation model after correcting for this observed structural anisotropy.

1 | INTRODUCTION

Silica glass fibers are known to exhibit birefringence which increases with applied axial tensile stress, such as during fiber drawing.[1,2] While some groups have investigated these effects in the fiber bulk, birefringence at or near the surface has not yet been explained. Birefringence can appear in glass either through residual stress or structural anisotropy. One example of the formation of residual stress in the glass surface is thermal tempering. Glass is strengthened by the formation of a surface compressive stress through rapidly cooling the glass from its softening point. Since thermal tempering requires the formation of a temperature gradient in the glass piece during cooling, it is unlikely to occur in glass fibers with a 125 μm diameter since the fiber is too thin to produce an adequate temperature distribution.[3] Structural anisotropy can occur in some organic glasses through alignment of chain structures. Among oxide glasses, phosphate glass fibers exhibit a high degree of structural birefringence through the orientation of chain structures.[4] Oxide glasses with a phase-separated structure can also exhibit birefringence when stretched due to elongation of the spherical microstructure into ellipsoidal shapes in the tensile direction.[5] In order to explain the observed birefringence of silica glass fibers, non-Newtonian viscous flow[6] and frozen-in viscoelasticity[7] have been proposed previously. These mechanisms may produce a uniform birefringence per sample thickness throughout a homogeneous silica glass fiber, but the reported birefringence per unit thickness in silica glass fibers appears to vary radially.[2,8,9]

Recently, a new method was discovered to strengthen glass fibers by introducing a residual compressive stress in the surface of glass fibers.[10] Subjected to a tensile stress for a short duration at a temperature far lower than the glass-transition temperature (T_g) in air, the glass surface undergoes rapid stress relaxation. The process is accelerated by small amounts of water vapor, and bulk stress relaxation is negligible at these low temperatures.[11,12] When the applied tensile stress is removed after cooling, the fiber acquires a surface compressive stress with nearly the same magnitude as the applied tensile stress, compensated by a low tensile stress inside the fiber bulk. The strengthening of fibers by this method has been demonstrated for silica glass,[13] E-glass,[14] and soda-lime silicate glass.[15] Fast surface stress relaxation has also been used to explain various mysterious phenomena related to the mechanical strength of glass, such as surface degradation of compressive stress made by ion-exchange,[16] crack arrest,[17] and the static fatigue limit.[18]

Fast surface stress relaxation would also produce non-uniform birefringence in glass fibers due to the resulting stress distribution. The existence of the surface residual stress of silica glass fibers by fast surface stress relaxation has previously been confirmed using shifts in the infrared reflection peak of strengthened fibers.[19] While surface stress relaxation and the resulting residual surface compressive stress have been demonstrated for silica glass fibers primarily at low temperatures (well below T_g) and short times in lab air, for example, 200ºC-500ºC in 60 seconds for silica glass, the same phenomenon is likely to occur at the higher temperatures in an even shorter time duration during fiber drawing. At higher temperatures, however, the effect is in concert with bulk stress relaxation as well as structural relaxation.[12] In the present research, the radial distribution of the birefringence of silica glass fibers is measured using a polarizing microscope and compared with a theoretical model based upon fast surface stress relaxation.

2 | EXPERIMENTAL PROCEDURE

Silica glass fibers with a 125 μm diameter are widely used for optical communications. Most commercial optical fibers consist of a core of about 8 μm in diameter with a slightly higher refractive index as well as a surrounding cladding with lower refractive index for a total of 125 μm. This core-cladding structure can produce residual stress due to the differences in glass compositions and properties of the glasses involved.[20] In order to simplify the birefringence observation and analysis, a coreless silica glass fiber with the same diameter as a commercial optical fiber made of Suprasil II (Heraeus Quartz Inc) was analyzed in the current experiments. The silica glass contains 1200wt. ppm OH, 0.1 wt. ppm Al, with all other impurities less than 0.05 wt. ppm. The glass-transition temperature was estimated to be ~952℃-1006ºC.[21–25]

Fibers were observed under a polarizing microscope (Nikon Eclipse, LV-100 NPOL) with an attached CMOS camera. Fibers were immersed in index-matching fluid matching the fiber surface index (Cargille immersion oil, n = 1.459) and placed with the fiber axis at 45º to both polarizer and analyzer in a cross-polarization configuration. The index of the immersion oil is accurate at 25ºC, with a deviation of −3.7e-4 per degree. The lab environment was kept within 2 degrees of this temperature. A conventional halogen light source with a $\lambda = 546$ nm interference filter (green) was used (see Figure 1A). Functions of the optical elements of the microscope are explained briefly in Figure

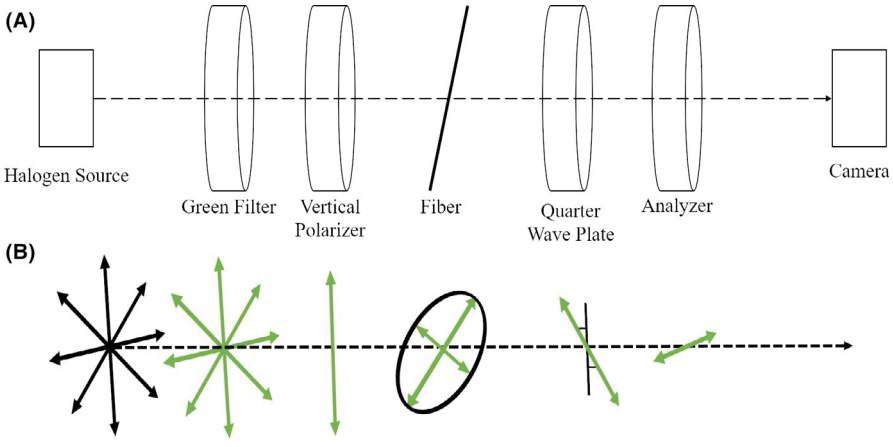

FIGURE 1 A, Schematic of relevant optical elements in the microscope and (B) outgoing light polarization following each component. Randomly polarized light is first filtered to 546 nm green light before becoming linearly polarized. This linearly polarized light passes through the fiber and is rendered elliptically polarized, with a fast (ordinary) and slow (extraordinary) component related to the retardance. This light is again converted back to linearly polarized light at a new angle via quarter wave plate. The angle can be determined as a function of analyzer angle, as intensity is minimized when the analyzer is perpendicular to the quarter wave plate output. This minimized intensity is measured via the attached camera to calculate the retardance at a given point in the fiber

1B. With the focal plane positioned in the center of the sample, 25 images were captured, and the measured intensity was averaged to mitigate noise. Relative intensity was analyzed using the greyscale values of the captured images, with an average standard deviation of 0.3% arising from the sensitivity of the camera. The fiber intensity profile was measured on a line perpendicular to the fiber drawing tension axis, which was used to define the x axis as perpendicular to the microscope image plane and fiber draw axis. Fifty such fiber profiles were averaged from this image using 0.17 μm increments (the pixel resolution of the camera, roughly half the spatial resolution of the microscope optics) to mitigate the effect of surface dust or other noise. A quarter wave plate was used in order to make quantitative measurements of retardance via the Sénarmont method.[26,27] This wave plate is paired to the green filter such that the retardance within the filter's wavelength is $\lambda/4$. The accuracy of the wave plate is assumed to be significantly higher than the error from the analyzer rotation. The quarter wave plate converts the elliptically polarized light resultant from the birefringent sample into linearly polarized light. This linearly polarized light has a retardance proportional to the angle of polarization that exits the wave plate.[28] Rotation of the analyzer allows for this resultant polarization angle to be quantified for the incident light wavelength: when the analyzer's polarization is perpendicular to the light exiting the quarter wave plate, intensity is minimized.

This method and equipment are similar to those used previously by other groups.[29–32] Retardance, $\Delta(x)$, is proportional to the refractive index difference and path length in a birefringent material:

$$\Delta(x) = (n_e - n_o) \cdot t(x), \tag{1}$$

where n_e is the refractive index of the extraordinary ray, n_o is that of the ordinary ray, and $t(x)$ is the local sample thickness along a vertical path at horizontal position, x. This index difference, a consequence of the material's response to incident polarized light, produces elliptically polarized light which varies as a function of x position along the fiber. The retardance is related to the stress by the stress-optic law:

$$\Delta(x) = C \cdot \sigma_{res}(x) \cdot t(x) \tag{2}$$

where C is the stress-optic coefficient of the material and σ_{res} is the residual axial stress. Many glasses including silica glass exhibit a positive stress-optical effect (exhibiting $n_e > n_o$) under tensile stress. Thus tensile stress which is defined positive, produces positive retardance. In literature on glass strengthening by residual surface compressive stress, it is customary to plot the surface compressive stress in positive y axis. Thus, in this study, $-\Delta(x)$, which corresponds to net axial compressive stress, will be plotted on the positive y axis as a function of fiber x position.

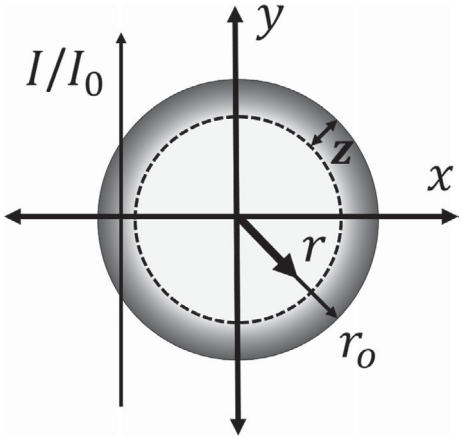

FIGURE 2 Schematic of fiber geometry in relation to incoming microscope light as described in Equation (3). Coordinates as defined here are used throughout the work, including the appendix. I/I_0 is the relative intensity of light as measured by the microscope camera, x and y are the horizontal and vertical directions in the fiber cross section, r is an interior radial position in the fiber, $r_0 = 62.5$ μm is the radius of the fiber, and z is the characteristic depth of surface stress relaxation

The Sénarmont method allows a connection to be made between incident wavelength, relative intensity, and the analyzer angle relative to the fixed polarizer. Intensity measured by the camera can be shown to be a function of analyzer angle and local retardance of the material.[33]

$$\frac{I(x)}{I_0} = \frac{1}{2} - \frac{1}{2}\cos(\delta(x) - 2\theta), \tag{3}$$

where I/I_0 is the relative intensity of the light measured by the camera, θ is the angle of the analyzer (with a range of $\pm 180°$) relative to its initial position perpendicular to the polarizer, and δ is the phase shift, or relative retardation, of the cosine function. The retardance, which is essentially a phase shift of the intensity curve given by Equation (3), may be expressed in nanometers instead of degrees of relative retardation by dimensional conversion:

$$\Delta(x) = \frac{\lambda}{180°} \cdot \frac{\delta(x)}{2}, \tag{4}$$

where λ is the wavelength corresponding to the filter and paired quarter wave plate.

From Equation (3), $\frac{I}{I_0}$ is minimized when

$$\delta = 2\theta \tag{5}$$

as shown by Jessop.[27] This solution provides the conversion factor between analyzer angle and relative retardation. A complete derivation for Equation (3) has been performed by Mori and Tomita for a cylinder, the fiber geometry.[34]

If a flat plate of glass with a uniform stress were examined in this manner, a single relative retardation value of δ would exist that corresponds to the analyzer angle θ at which the measured intensity is minimized. The only difference in the case of a fiber is the retardance is now affected by the difference in path length (fiber geometry) and the change in stress through that path (in this case, surface compression and interior tension). Figure 2 shows how the radial position of the fiber can affect the measured retardation, as each x position produces a corresponding δ value, depending on the sum of tensile and compressive stresses through the fiber cross section at points of constant x.

The relative intensity profile of the fiber was measured from the acquired images using a second-order polynomial least squares fit in order to estimate the value of analyzer θ to a greater accuracy than the measurement interval of $0.2 \pm 0.05°$. The minimum intensity as described in Equation (3) was determined at each pixel of the profile as a function of θ. Thus the minimum intensity angle could be mapped to its x position on the fiber. Relative retardation δ was calculated using Equation (3) at every point, then converted to retardance using Equation (4). The retardance measurement error depends mainly on the accuracy of the analyzer rotation, which is performed by hand using 0.1-degree Vernier marks. Error in measurement is conservatively estimated to be about half of the increment, corresponding to a retardance error of about 0.15 nm based on Equation (4). The measurement error and spatial resolution are used as the error bounds for the figures in this work, as will be shown in Figure 7(B), the only figure in which the error is noticeably larger than the data points.

This procedure can produce retardance measurements at every point captured by the microscope, allowing for both x position profiles as well as full two-dimensional retardance plots (see Figure 3). The resulting retardance profiles were then fit to the proposed model for retardance from surface stress relaxation (see Appendix).

In order to confirm the trend of increasing surface stress with increasing applied load during strengthening by surface stress relaxation at low temperatures, fibers were heated to 200ºC for 60 seconds in air while under a tensile load ranging from 0 to 2.0 GPa. Fibers annealed at 1200ºC for 1 hour then furnace cooled were found to have negligible retardance. Additionally, some as-received fibers were progressively etched by immersion in a 48% HF solution. Etching took place over various lengths of time (20 seconds to 6 minutes) to remove between 0.5 and 4.0 μm of the surface layer. The retardance of the processed fibers were then compared to the as-received fibers, which consisted of evaluating the values of the effective depth, z, and the estimated compressive stress at the fiber surface via the developed model.

3 | RESULTS

The average measured retardance for as-received silica glass fibers was obtained (see Figure 3). Both the birefringence photograph and the measured retardance profile are shown.

The measured retardance was compared with the curves generated from the surface stress relaxation model shown in Figure A1 and Equation (A11) in the Appendix. In Figure A1, residual stress profiles produced by surface stress relaxation are shown using the applied tensile stress, σ_{applied}, and the surface relaxed layer thickness, z, as parameters. The measured retardation profile shown in Figure 3 was compared with the best fit theoretical model. By fitting the proposed model to the measured data and the applied stress, and using a literature value for the stress optic coefficient C (3.19 Brewster, $\left[10^{-6}\,\text{MPa}^{-1}\right]$),[35] estimates of this z value (μm) and σ_{applied} were selected to obtain the best fit, especially in the fiber surface region. The resultant curve was compared to the measured data as shown in Figure 4.

The general features of the measured retardance of these fibers agreed with the predicted values using the surface stress relaxation model, both exhibiting high compressive stresses on the surface of the fibers with the shallower tensile stress zone observed in the middle part of the fibers. However, the details of the measured and predicted curves showed some systematic difference in the interior of the fiber. The balance of forces within the fiber predicts that the sum of the retardation from residual stresses of the fiber should be zero, with the total integrated compressive stress (area above the zero retardance line) cancelling the total integrated tensile stress (area below the zero line). The measurement, however, appears to have a greater contribution of "tensile stress" near the center of the fiber (below the zero retardance line) equivalent to ~16-20 MPa. The effect is consistent across samples. The extra retardance greatly surpasses the error of the measurement (±0.15 nm) near the center of the fiber, while it approaches the error range near the surface. This extra "tensile stress" appears to be related to an anisotropic structure due to previous uniaxial stress application.[36,37] The model parameters were first fit to estimate the surface stress relaxation contribution followed by a correction factor k for the bulk anisotropy:

$$\Delta(x) = \int_{y_{min}=-\sqrt{r_0^2-x^2}}^{y_{max}=\sqrt{r_0^2-x^2}} C \cdot \{\sigma_{res}(x,y) + k\}\,\mathrm{d}y. \tag{7}$$

Equation (7) is thus a modification of Equation (A11) to include uniform structural anisotropy. The correction factor is within the integral, rendering it proportional to the fiber path length.

In order to quantitatively isolate this additional component of structural anisotropy, the retardance of the silica

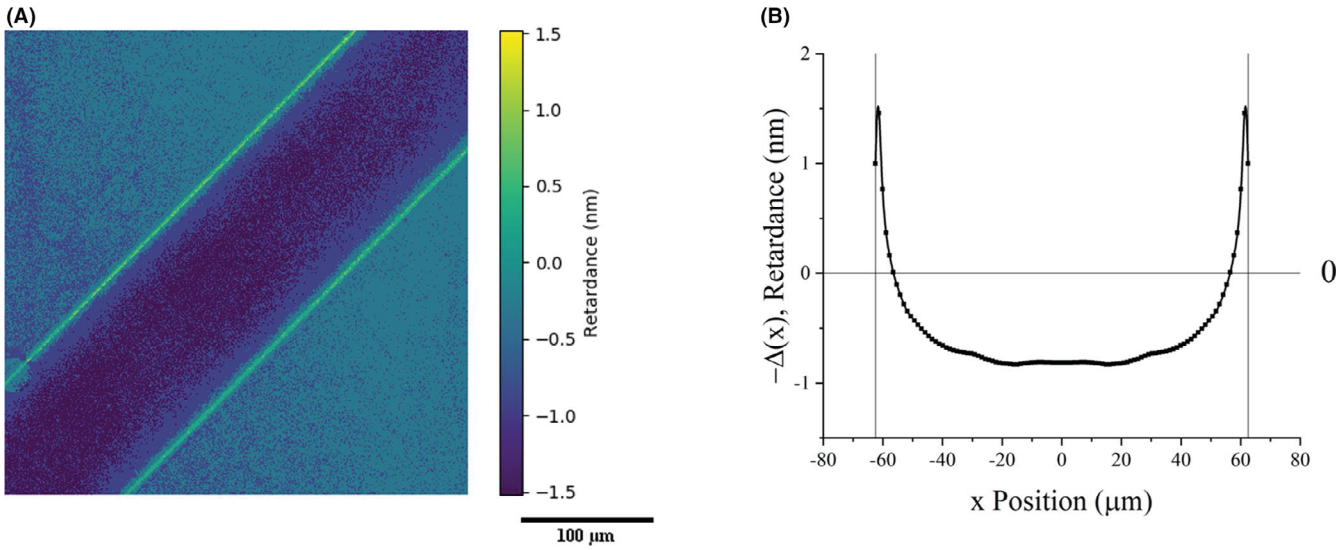

FIGURE 3 A, Map of as-received fiber retardance created using the same process as the profile measurement extended to the full microscope field of view. B, measured retardance profile of as-received fiber, with fiber surface x position and the zero point of retardance indicated in vertical and horizontal guidelines, respectively. Points are the measured data while the line is a guide to the eye

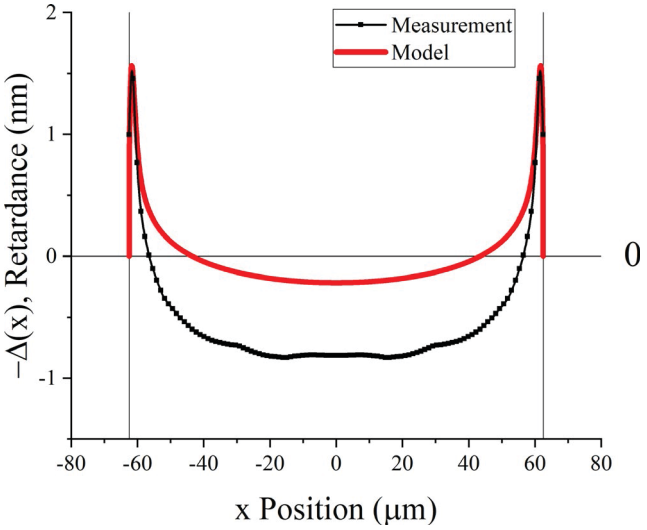

FIGURE 4 Model fit of as-received fiber retardance measurement, showing excess of internal "tensile stress."

glass fiber based upon the surface stress relaxation model was subtracted from the measured retardance. First, the measured retardance of the fiber surface was fit to the theory by adjusting the value of z and the applied stress, σ_{applied}. The residual stress is determined primarily by the applied tensile stress at the treatment temperature (see Equation (A8)). The model prediction of the retardance due to the residual stress caused by the surface stress relaxation can thus be obtained. By subtracting the model retardance from the experimental retardance (difference of two lines in Figure 4, the remaining experimental retardance due to structural anisotropy is shown in Figure 5(B), together with the color map of the corresponding fiber (Figure 5(A)). The surface residual stress due to surface stress relaxation can be eliminated at a temperature far lower than the glass transition temperature, while the birefringence due to structural anisotropy requires much higher temperature. The heat-treatment at 650℃ for 10 minutes in air is appropriate to eliminate the former while leaving the latter intact.

These analyses were conducted for all the measured retardance profiles of glass fibers, including those given low-temperature tensile stress treatment. In this case, applied stress parameter, σ_{applied}, was the stress employed in the tensile stress treatment. All the parameters generated through this analysis are shown in Table 1. When these two contributions to the birefringence were combined, the results agreed with the measured retardance as shown in Figure 6.

Thus, the discrepancy between the experimental retardance and the model based upon surface stress relaxation can be attributed to structural anisotropy, which corresponds to "tensile stress." The constant k, introduced to represent uniform structural anisotropies, is listed in Table 1 alongside the other fitting parameters as well as estimates of the surface residual stress. Stress units were used for the anisotropy to show what magnitude of tensile stress would produce a comparable retardance. The same table lists the fitting parameters for the measured retardance of fibers given strengthening treatment at a low temperature, 200ºC, for 60 seconds in air under various tensile stresses as well as zero stress.

Figure 7A shows the collective change of birefringence profiles of silica glass fibers by the low-temperature strengthening treatment and Figure 7B shows, in magnified scales, a part of Figure A1 indicating the detailed change of surface

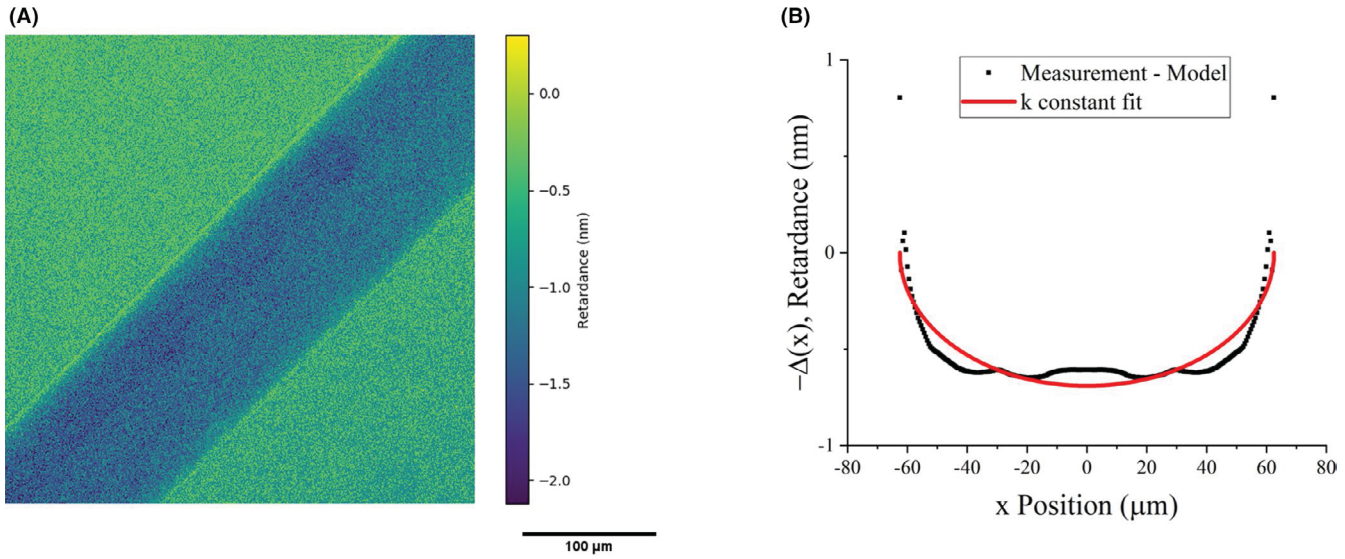

FIGURE 5 A, A map generated from a heat-treated fiber (650°C, 10 min at rest in lab air), revealing structural anisotropy in the fiber interior. B, Corresponding retardance profile

TABLE 1 Estimated model parameters, ±95% confidence bounds, and surface residual stress estimate as defined in the Appendix.

Fiber Condition	z [µm]	$\sigma_{applied}$[GPa] (tensile)	k [MPa] (tensile)	$\sigma_{res,surface}$[GPa] (compressive)
As-Received (Figure 3)	0.68 ± 0.07	0.45 ± 0.4*	16.5 ± 0.2	0.43 ± 0.02
Heat Treat, 0 GPa	0.71 ± 0.09	0.29 ± 0.15*	17.0 ± 0.2	0.27 ± 0.02
0.5 GPa	0.47 ± 0.07	0.5	19.6 ± 0.2	0.47 ± 0.02
1.0 GPa	0.29 ± 0.02	1.0	17.9 ± 0.2	0.97 ± 0.02
1.5 GPa	0.18 ± 0.01	1.5	18.3 ± 0.2	1.47 ± 0.02
2 GPa	0.22 ± 0.01	2.0	16.3 ± 0.2	1.97 ± 0.02

*Value estimate from fit; applied stress unknown or negligible during treatment

compressive stress profiles. These results show that surface stress profiles are sensitive to low temperature (200ºC) tensile stress treatment conducted for a short time (60 seconds in air), supporting that the observed surface stress is originated from the surface stress relaxation. The surface compressive stress decreased under low tensile stress, while it increases under higher tensile stress. This is reasonable since the surface compressive residual stress produced is nearly equal to the applied tensile stress.[10,11] The change of the depth z of the surface residual stress due to surface stress relaxation is known to increase with the square root of the treatment time. There is an apparent trend of decreasing relaxation depth with increasing applied stress. Despite being near the resolution limitations of the measurement, the fitting error for this trend (about 10%) is lower than the trend itself. This may merit further investigation involving longer heat treat times to determine if the same trend is also observed for larger values of z.

The compressive stress peaks present in the as-received fiber must be the result of a surface stress relaxation phenomenon, as the peaks are significantly decreased proportional to progressive etching (see Figure 8), while the retardance in the interior of the fiber was affected much less so. This surface etching of the sample accentuates the imbalance between the surface compressive stress and the interior tensile stress and demonstrate the presence of interior structural anisotropy. With the removal of surface compression, much of the interior structural anisotropy-originated "tension" remains. Here the observed fluctuation of the retardance curves in Figure 8B may be due to the magnified scale of retardance with the corresponding magnification of error range. Since this fluctuation appears to be symmetric with respect to the central fiber axis, there may be a small fluctuation of structural anisotropy.

4 | DISCUSSION

The measured retardance of as-received silica glass fibers agrees with the surface stress relaxation model well, except

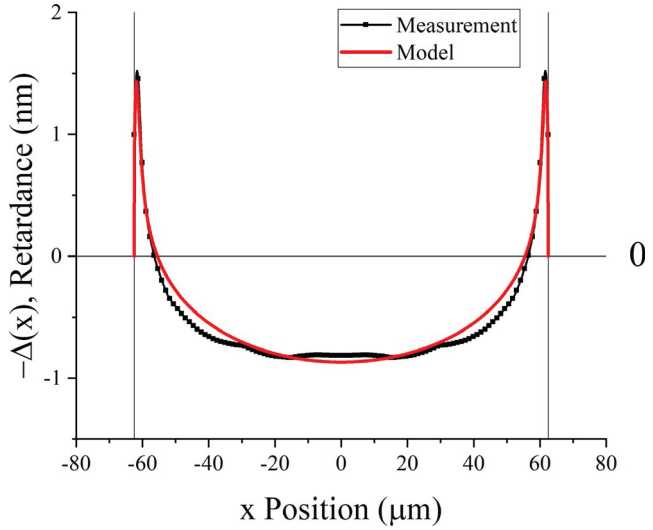

FIGURE 6 Resultant fit between the combined retardance of residual stress due to surface stress relaxation and structural anisotropy and the measurement

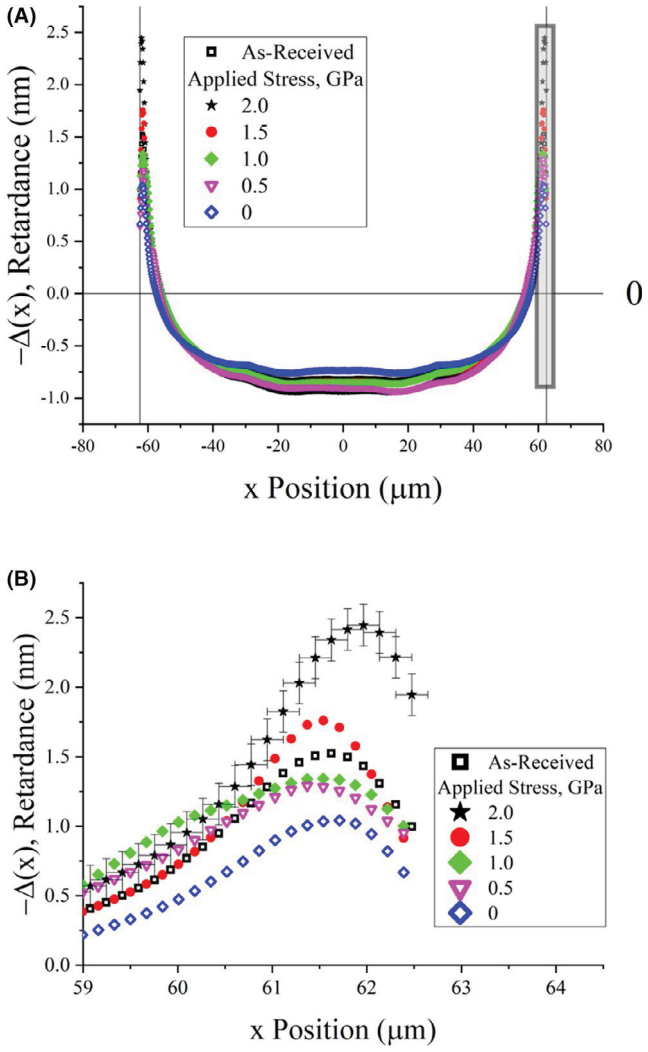

FIGURE 7 A, Strengthening via surface stress relaxation using various applied stresses and (B) an enlarged region of interest as indicated in (A), with error bars on the highest curve representative of those on each curve. Note that the peak height increases systematically with increasing applied stress during heat treatment

for a finite deviation from the theory which appears to be a nearly uniform structural anisotropy in the fiber. This deviation in the interior of fibers likely resulted from structural anisotropy created at high temperature, as the low-temperature tensile stress treatment at 200ºC for 60 seconds in air appears to have little effect. This is seen in the magnitude of the correction factor k in Table 1, which seems to be constant and independent of the low-temperature strengthening treatment, approximately 17.6 ± 1.3 MPa. This excess retardance corresponding to "tensile stress" cannot be a result of residual stress, as there is no corresponding compressive stress to balance the forces. Because this interior retardance is nearly constant throughout the low-temperature strengthening heat treatments, the retardance is a result of bulk structural anisotropy, which requires higher temperatures or longer heat-treatment times to be significantly affected and is clearly separate from the surface stress relaxation mechanism.[2]

Although the anisotropy can be fit alongside the compressive and tensile stresses within the fiber using the same stress optic coefficient, as is done in Equation (7), this does not imply the stress optic coefficient is necessarily identical for both contributions. More work would be necessary to determine if the stress optic coefficient itself is sensitive to the fiber drawing conditions, although this is unlikely. Others have found that in as-received single-mode fibers containing a core with a doped surface layer, the stress optic coefficient appears constant through the cross section.[36]

The obtained k values in Table 1 are nearly constant, independent of the low-temperature strengthening process, indicating that the structural anisotropy represented by k was unaffected by the change of residual stress. This constant value of k supports the notion that structural anisotropy is a bulk phenomenon which was produced during the fiber drawing process at higher temperatures. The 200ºC heat treatments are unable to affect the structural anisotropy in 60 seconds since they take place so far below T_g, where bulk structural relaxation occurs readily.

Similarly, progressive etching results in a decrease and ultimately a removal of surface compressive stress. The interior "tensile stress" retardance decreases to a lesser degree by the etching process but does not vanish with the disappearance in surface compression. This also seems to suggest a bulk retardance resulting from structural alignment due to the fiber drawing process and not simply a compensating tensile stress for the surface compression.

A similar structural anisotropy was observed in silica glass subjected to uniaxial stresses, both compressive stress and tensile

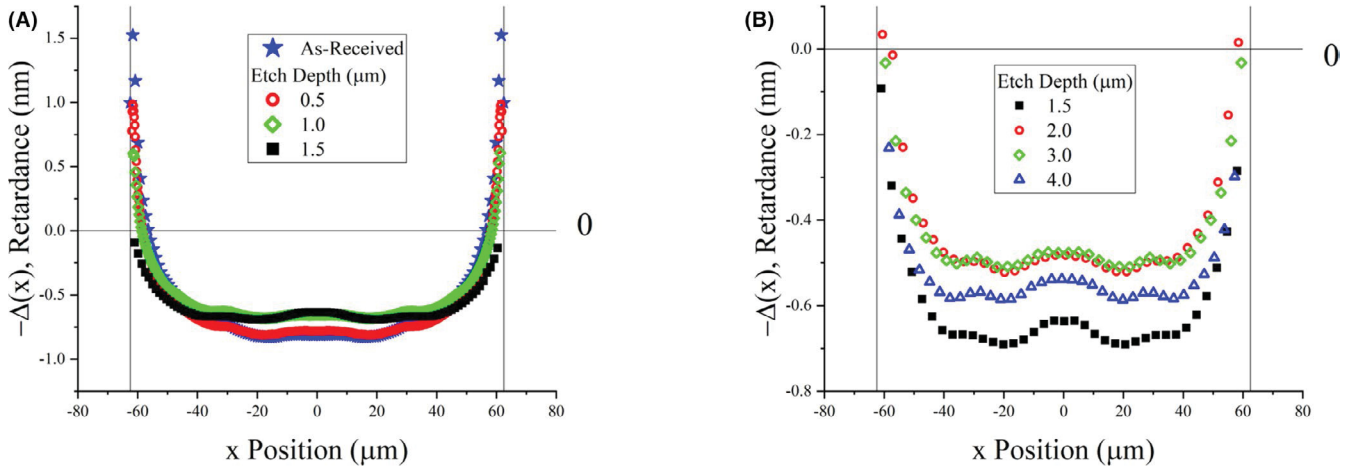

FIGURE 8 Progressive surface etching, with retardance zero point and fiber surface indicated with thin guidelines. A, Surface compression peaks drop with etching, leaving a slightly smaller remnant retardance. B, Further etching past 1.5 μm results in little change to bulk retardance, implying a physical origin connected to fiber geometry. Note that the scale of y axis of (B) is magnified by about three times compared with (A)

stress.[37,38] Sato et al.[37] observed a shift of first sharp diffraction peak (FSDP) position of X-rays, a measure of the intermediate order in glass corresponding to the arrangement of tetrahedral units, in silica glass subjected to uniaxial compressive stress. This shift remained after the compressive stress was removed. Furthermore, the position of the FSDP was a function of the sample orientation with respect to the uniaxial stress, meaning that the shift was not a result of simple uniform densification, but was in fact anisotropic.

Earlier, Murach and Bruckner[1] observed frozen-in birefringence in fine silica fibers with diameters ranging from ~10-60 μm of three different silica glasses drawn at high temperatures ~2350ºC-2430ºC. They measured the magnitude of birefringence of the bundle of these fibers and found a greater birefringence in the fiber when the silica glass fibers were drawn under a higher stress or when the fibers had a higher water content.[1]

Observed birefringence in fibers is often attributed to frozen-in viscoelasticity.[39] It is known that the delayed elastic component in a viscoelastic material is absent when a glass has only one relaxation time at a given temperature or equivalently when the KWW exponent, β, of relaxation is unity.[40] High-purity silica glasses, including silica glass containing Cl, have a single relaxation time as can be seen from the absence of the memory effect.[41,42] For these glasses, there can be no frozen viscoelasticity. When silica glasses contain increasing impurity contents of water or fluorine, glasses exhibited greater memory effect, and thus a widening distribution of relaxation times.[41] This distribution of relaxation times is thought to correspond to local compositional fluctuations, which could align under stress to produce the observed structural anisotropy.[43]

Glasses containing water impurities exhibited large internal friction or viscoelasticity: on a per mole basis, in both phosphate[44] and silicate glasses[45], water in glass exhibited an internal friction loss peak which is greater in magnitude than those of alkali or alkaline ions in the same glass by a factor of 100. The previously mentioned increased birefringence with increased OH content by Murach and Bruckner[1] suggests greater frozen viscoelasticity (or internal friction peak) due to OH impurity for silica glass as well. In the method of birefringence measurement employed by Murach and Bruckner[1], who analyzed a bundle of several fibers to produce an average value, residual stress contribution from surface stress relaxation would not be detected due to the cancellation of compressive stress with tensile stress. Furthermore, their birefringence data do not extrapolate to zero when the water impurity content was extrapolated to zero. This is probably due to the entry of the additional water impurity into silica glass fibers during the fiber drawing process, since they used a hydrogen-oxygen burner.[46,47]

It is thus suggested that the observed structural anisotropy in the fibers employed in the present study, Suprasil II, which contains 1200 ppm OH, can be attributed to the water impurity. The large effect of small water content in silica glasses has been attributed to concentration fluctuation of SiO_2-H_2O system.[43]

5 | CONCLUSION

Birefringence observed at the surface of silica glass fibers can be explained by surface stress relaxation. The fiber undergoes fast surface stress relaxation enhanced by water vapor in air during the fiber drawing process. Similar retardance profiles can be observed in fibers undergoing low-temperature heat treatments in air under tension, resulting in retardance proportional to the applied tensile load. Removal of the fiber surface via etching results in a decrease in the observed retardance, by removal

of the surface compressive stress. Remaining retardance after etching is likely the result of structural alignment from the fiber drawing process, produced by viscoelastic alignment of regions with small compositional fluctuations.

ACKNOWLEDGMENTS

This research was supported by the NSF grant DMR-1713670 and Corning, Inc

ORCID

Bronson D. Hausmann https://orcid.org/0000-0003-1448-3392

REFERENCES

1. Murach J, Brückner R. Preparation and structure-sensitive investigations on silica glass fibers. J Non-Cryst Solids. 1997;211:250–61.
2. Durr F, Limberger HG, Salathé RP, Yablon AD.Inelastic strain birefringence in optical fibers. 2006 Optical Fiber Communication Conference and Exposition and The National Fiber Optic Engineers Conference. Anaheim, CA: IEEE; 2006
3. Rongved L, Kurkjian CR, Geyling FT. Mechanical tempering of optical fibers. J Non-Cryst Solids. 1980;42:579–84.
4. Brückner R, Murach J, Hao S. Generation and relaxation of flow birefringence of high-viscous alkali phosphate glass melts. J Non-Cryst Solids. 1996;208:228–36.
5. Takamori T, Tomozawa M. Birefringence and microstructure of anisotropic borosilicate glasses. J Am Ceram Soc. 1976;59(9–10):377–9.
6. Brückner R, Yue Y. Non-Newtonian flow behaviour of glass melts as a consequence of viscoelasticity and anisotropic flow. J Non-Cryst Solids. 1994;175:118–28.
7. Yablon AD, Yan MF, DiGiovanni DJ, Lines ME, Jones SL, Ridgway DN, et al. Frozen-in viscoelasticity for novel beam expanders and high-power connectors. J Light Technol. 2004;22(1):16-23.
8. Wissuchek DJ, Ponader CW, Price JJ. Analysis of residual stress in optical fiber. In: Matthewson MJ , editor. Optical fiber reliability test, Vol. 3848. Bellingham, WA: International Society for Optics and Photonics, 1999; p. 34–44.
9. Hutsel MR, Ingle R, Gaylord TK. Accurate cross-sectional stress profiling of optical fibers. Appl Opt. 2009;48(26):4985–95.
10. Tomozawa M, Lezzi PJ, Hepburn RW, Blanchet TA, Cherniak DJ. Surface stress relaxation and resulting residual stress in glass fibers: a new mechanical strengthening mechanism of glasses. J Non-Cryst Solids. 2012;358:2650–62.
11. Aaldenberg EM, Aaldenberg JS, Blanchet TA, Tomozawa M. Surface shear stress relaxation of silica glass. J Am Ceram Soc. 2019;102(8):4573–82.
12. Tomozawa M, Davis KM, Seaman JH, Aaldenberg EM. The origin of anomalous water diffusion in silica glasses at low temperatures. J Am Ceram Soc. 2017;100(10):4548–61.
13. Lezzi PJ, Xiao QR, Tomozawa M, Blanchet TA, Kurkjian CR. Strength increase of silica glass fibers by surface stress relaxation: a new mechanical strengthening method. J Non-Cryst Solids. 2013;379:95–106.
14. Lezzi PJ, Seaman JH, Tomozawa M. Strengthening of E-glass fibers by surface stress relaxation. J Non-Cryst Solids. 2014;402:116–27.
15. Lezzi PJ, Tomozawa M. An overview of the strengthening of glass fibers by surface stress relaxation. Int J Appl Glass Sci. 2015;6(1):34–44.
16. Seaman JH, Lezzi PJ, Blanchet TA, Tomozawa M. Degradation of ion-exchange strengthened glasses due to surface stress relaxation. J Non-Cryst Solids. 2014;403:113–23.
17. Seaman JH, Lezzi PJ, Blanchet TA, Tomozawa M. Modeling slow crack growth behavior of glass strengthened by a subcritical tensile stress using surface stress relaxation. J Am Ceram Soc. 2015;98(10):3075–86.
18. Seaman JH, Blanchet TA, Tomozawa M. Origin of the static fatigue limit in oxide glasses. J Am Ceram Soc. 2016;99(11):3600–9.
19. Lezzi PJ, Tomozawa M, Hepburn RW. Confirmation of thin surface residual compressive stress in silica glass fiber by FTIR reflection spectroscopy. J Non-Cryst Solids. 2014;390:13–8.
20. Paek UC, Kurkjian CR. Calculation of cooling rate and induced stresses in drawing of optical fibers. J Am Ceram Soc. 1975;58(7–8):330–5.
21. Agarwal A, Davis KM, Tomozawa M. A simple IR spectroscopic method for determining fictive temperature of silica glasses. J Non-Cryst Solids. 1995;185:191–8.
22. Kuzuu N. Characteristic temperature, fictive temperature. In: Kawazoe H, editor. Practical handbook for amorphous siliceous materials. Tokyo: Realize Inc., 1999; p. 91–8.
23. Kirchhof J, Unger S, Dellith J. Viscosity of fluorine-doped silica glasses. Opt Mater Express. 2018;8(9):2559–69.
24. Ohashi M, Tateda M, Tajima K, Shiraki K. Fluorine concentration dependence of viscosity in F-doped silica glass. Electron Lett. 1992;28(11):1008–10.
25. Smith CM, Moore LA. Properties and production of F-doped silica glass. J Fluor Chem. 2003;122(1):81–6.
26. Goranson RW, Adams LH. A method for the precise measurement of optical path-difference, especially in stressed glass. J Frankl Inst. 1933;216(4):475–504.
27. Jessop HT. On the Tardy and Sénarmont methods of measuring fractional relative retardations. Br J Appl Phys. 1953;4(5):138–41.
28. Aben H, Guillemet C. Photoelasticity of glass. Berlin: Springer 1993; p. 51–67.
29. Chu PL, Whitbread T. Measurement of stresses in optical fiber and preform. Appl Opt. 1982;21(23):4241–5.
30. Hutsel MR, Ingle RR, Gaylord TK. Technique and apparatus for accurate cross-sectional stress profiling of optical fibers. IEEE Trans Instrum Meas. 2010;60(3):971–9.
31. Park Y, Ahn T-J, Kim YH, Han W-T, Paek U-C, Kim DY. Measurement method for profiling the residual stress and the strain-optic coefficient of an optical fiber. Appl Opt. 2002;41(1):21–6.
32. C14 Committee. ASTM F218–13 Standard test method for measuring optical retardation and analyzing stress in glass. West Conshohocken, PA: ASTM International, 2013.
33. Pedrotti FL, Pedrotti LM, Pedrotti LS. Introduction to optics. 3rd ed. Upper Saddle River, NJ: Pearson/Prentice Hall, 2007.
34. Mori A, Tomita R. Semi-automated Sènarmont method for measurement of small retardation. Instrum Sci Technol. 2015;43(4):379–89.
35. Lagakos N, Mohr R, El-Bayoumi OH. Stress optic coefficient and stress profile in optical fibers. Appl Opt. 1981;20(13):2309–13.
36. Acheroy S, Merken P, Ottevaere H, Geernaert T, Thienpont H, Berghmans F. Influence of measurement noise on the determination

of the radial profile of the photoelastic coefficient in step-index optical fibers. Appl Opt. 2013;52(35):8451–9.
37. Sato T, Funamori N, Yagi T. Differential strain and residual anisotropy in silica glass. J Appl Phys. 2013;114(10):103509.
38. Champagnon B, Degioanni S, Martinet C. Anisotropic elastic deformation of silica glass under uniaxial stress. J Appl Phys. 2014;116(12):123509.
39. Yablon AD. Optical and mechanical effects of frozen-in stresses and strains in optical fibers. IEEE J Sel Top Quantum Electron. 2004;10(2):300–11.
40. Scherer GW. Experimental studies of relaxation and creep. In: Relaxation in glass and composites. Malabar, FL: Krieger, 1992; p. 41–6.
41. Tomozawa M, Koike A, Ryu S-R. Exponential structural relaxation of a high purity silica glass. J Non-Cryst Solids. 2008;354:4685–90.
42. Koike A, Ryu S-R, Tomozawa M. Adequacy test of the fictive temperatures of silica glasses determined by IR spectroscopy. J Non-Cryst Solids. 2005;351:3797–803.
43. Aaldenberg EM, Tomozawa M. Composition fluctuations in silica glass containing water. Am Ceram Soc Bull. 2019;98(5):34–5.
44. Day DE, Stevels JM. Effect of dissolved water on the internal friction of glass. J Non-Cryst Solids. 1974;14:165–77.
45. Reinsch S, Müller R, Deubener J, Behrens H. Internal friction of hydrated soda-lime-silicate glasses. J Chem Phys. 2013;139(17):174506.
46. Thomas GA, Shraiman BI, Glodis PF, Stephen MJ. Towards the clarity limit in optical fibre. Nature. 2000;404(6775):262–4.
47. Kim BH, Han SR, Paek U-C, Han W-T. Diffusion of OH in optical fiber preform by oxy-hydrogen burner. J Non-Cryst Solids. 2004;349:248–53.

How to cite this article: Hausmann BD, Miller PA, Aaldenberg EM, Blanchet TA, Tomozawa M. Modeling birefringence in SiO_2 glass fiber using surface stress relaxation. *J Am Ceram Soc*. 2020;103:1666–1676. https://doi.org/10.1111/jace.16900

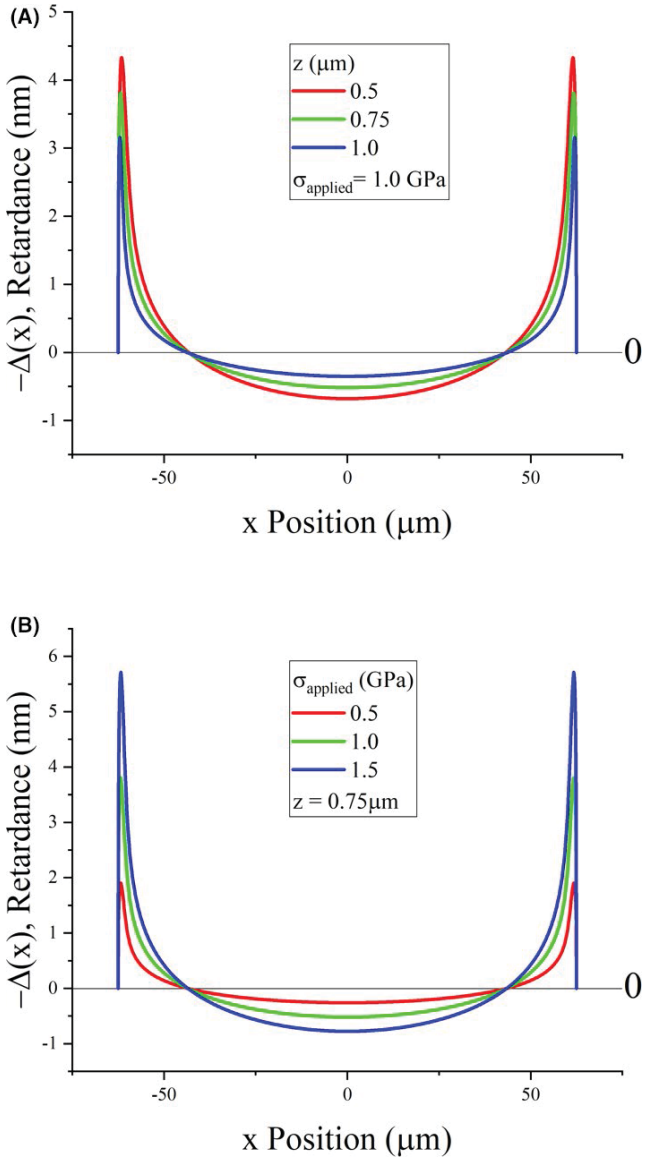

FIGURE A1 A, Plot of retardance with variations in parameter z with $\sigma_{applied}$ fixed at 1.0 GPa (B) as well as variations in parameter $\sigma_{applied}$ with z fixed at 0.75 μm. The plots shown use the stress optic coefficient of Suprasil II[35]

APPENDIX
BIREFRINGENCE DUE TO SURFACE STRESS RELAXATION

A uniform uniaxial tensile stress is imposed on the fiber either during the manufacturing process or in the lab via uniform applied stress, which is correlated with a uniform strain in the material:

$$\sigma_{applied} = E \cdot \varepsilon_{applied}. \quad \text{(A1)}$$

Due to the surface stress relaxation, the originally uniform applied tensile stress, $\sigma_{applied}$, changes to a relaxed stress, σ_{relax}, with a thin surface layer of thickness z losing the stress by a diffusion-controlled process, promoted by moisture in the atmosphere:

$$\sigma_{relax}(r,z) = \sigma_{applied} \cdot \left[1 - \text{erfc}\left(\frac{r_0 - r}{2z}\right)\right], \quad \text{(A2′)}$$

$$\sigma_{relax}(r,z) = \sigma_{applied} \cdot \text{erf}\left(\frac{r_0 - r}{2z}\right), \quad \text{(A2″)}$$

where r_0 is fiber radius, r is radial position within the fiber, and z is the characteristic relaxation depth (see Figure 2). Note this model assumes that $z \ll r_0$ in order to approximate a planar diffusion at the fiber surface using the error function.[13] This depth can be related to the effective diffusivity

of surface stress relaxation, D, and the time of the heat treatment, t :

$$z = \sqrt{Dt}. \tag{A3}$$

With this relaxation, when the imposed axial strain is subsequently released, strain will spring back by some uniform $\Delta\varepsilon_{sb}$ resulting in a residual axial stress σ_{res} as $\sigma_{relax}(r)$ is reduced by $\Delta\sigma_{sb} = E\Delta\varepsilon_{sb}$:

$$\sigma_{res}(r,z) = \sigma_{relax}(r,z) - \Delta\sigma_{sb} \tag{A4}$$

This balance is radially symmetrical about the cross section of the fiber, and must also radially integrate to zero, $\int \sigma_{res} dA = 0$:

$$\int (\sigma_{applied} \cdot \mathrm{erf}\left(\frac{r_o - r}{2z}\right) - \Delta\sigma_{sb}) dA = 0. \tag{A5}$$

Considering the radial cross section:

$$\sigma_{applied} \cdot \int_0^{r_o} \mathrm{erf}\left(\frac{r_o - r}{2z}\right) 2\pi r dr - \Delta\sigma_{sb}\pi r_o^2 = 0. \tag{A6}$$

Solving for $\Delta\sigma_{sb}$ and substituting into Equation (A4), residual axial stress becomes a function of radial position:

$$\sigma_{res}(r,z) = \sigma_{applied}\left\{\mathrm{erf}\left(\frac{r_o - r}{2z}\right) - \frac{2}{r_o^2}\int_0^{r_o} \mathrm{erf}\left(\frac{r_o - r}{2z}\right) \cdot r dr\right\}. \tag{A7}$$

The integral has a closed-form solution resulting in the following residual stress profile:

$$\sigma_{res}(r,z) = \sigma_{applied} \cdot \left\{\mathrm{erf}\left(\frac{r_o - r}{2z}\right) - \left(\frac{2r_o z \cdot e^{-\frac{r_o^2}{4z^2}} + \sqrt{\pi} \cdot \left(r_o^2 + 4z^2\right) \cdot \mathrm{erf}\left(\frac{r_o}{2z}\right) - 4r_o z}{\sqrt{\pi} r_0^2}\right)\right\}. \tag{A8}$$

Birefringence (and thus retardance) is linearly proportional to stress, and can be expressed as follows:

$$d\Delta = C \cdot \sigma_{res}(r,z)\, dy, \tag{A9}$$

where C is the stress optic coefficient dy is a differential form of the path length. Thus, referring to the coordinates of Figure 1A, for any x position along the fiber profile:

$$\Delta(x) = \int_{y_{min}(x)}^{y_{max}(x)} C \cdot \sigma_{res}(r,z)\, dy, \tag{A10}$$

where Δ is retardance and dy gives the orientation of the path length parameter, which is expressed in the integral limits as a function of x position. $\sigma_{res}(r)$ can be converted to rectangular coordinates. The r term in Equation (A8) is simply replaced with $\sqrt{x^2 + y^2}$:

$$\Delta(x) = \int_{y_{min} = -\sqrt{r_0^2 - x^2}}^{y_{max} = \sqrt{r_0^2 - x^2}} C \cdot \sigma_{res}(x,y)\, dy. \tag{A11}$$

This result produces a retardance profile comparable to those expected from surface stress relaxation.[10] Figure A1 illustrates the result of this equation using different z and $\sigma_{applied}$ values.